http://dx.doi.org/10.5012/bkcs.2014.35.9.2726

In Situ-DRIFTS Study of Rh Promoted $CuCo/Al_2O_3$ for Ethanol Synthesis *via* CO Hydrogenation

Fang Li,[†,‡] Hongfang Ma,[†] Haitao Zhang,[†] Weiyong Ying,[†,*] and Dingye Fang[†]

[†]*Engineering Research Center of Large Scale Reactor Engineering and Technology, Ministry of Education, State Key Laboratory of Chemical Engineering, East China University of Science and Technology, Shanghai 200237, China*
[*]*E-mail: wying@ecust.edu.cn*
[‡]*School of Biochemical Engineering, Anhui Polytechnic University, Wuhu, 241000, Anhui, China*
Received December 29, 2013, Accepted May 14, 2014

The promoting effect of rhodium on the structure and activity of the supported Cu-Co based catalysts for CO hydrogenation was investigated in detail. The samples were characterized by DRIFTS, N_2-adsorption, XRD, H_2-TPR, H_2-TPD and XPS. The results indicated that the introduction of rhodium to Cu-Co catalysts resulted in modification of metal dispersion, reducibility and crystal structure. DRIFTS results of CO hydrogenation at reaction condition (P=2 MPa, T=260 °C) indicated the addition of 1 wt % rhodium improved hydrogenation ability of Cu-Co catalysts. The ethanol selectivity and CO conversion were both improved by 1 wt % Rh promoted Cu-Co based catalysts. The alcohol distribution over un-promoted and rhodium promoted Cu-Co based catalysts obeys A-S-F rule and higher chain growth probability was got on rhodium promoted catalyst.

Key Words : Copper-cobalt, Rhodium, DRIFTS, CO hydrogenation, Ethanol

Introduction

Ethanol is an important industry material for the synthesis of acetic acid, beverage, essence, dyes, fuels and disinfectant, and has also been commercially used as an additive or a potential supplement for gasoline.[1] Direct synthesis of ethanol from syngas may complement the traditional microbial fermentation. However, the process has not been commercially implemented due to its lower transformation efficiency. Thus, various types of catalysts have been reported such as Rh based,[2,3] modified Cu based,[4,5] Mo based[6,7] and modified Fischer-Tropsch (F-T) catalysts.[8,9] Cu-Co based catalysts, as one of the most effective catalysts for higher alcohol synthesis, were patented in 1970s by the IFP. Recent reports mainly concentrated on un-promoted Cu-Co supported catalysts to get information about active sites, the interaction between copper and cobalt and so on.[10-14] It is widely accepted that Cu is responsible for non-dissociative activation of CO for insertion, while Co assists as active sites to dissociate CO.[15] Thus, various Cu-Co based supported catalysts were focused.

However, most of the catalysts are the un-promoted. As a result, excellent performance cannot be obtained. Recent studies indicated that the catalysts with outstanding properties were often promoted by more than three metals. Especially, the addition of noble metal usually displays excellent performance for the adsorption and spillover of hydrogen in F-T synthesis.[16] Mariane *et al.* found that the addition of 1 wt % ruthenium to Co/carbon nanotubes can increase the dispersion and decreasing the cobalt cluster size during F-T synthesis.[17] Surisetty *et al.* reported that the selectivity of ethanol for CO hydrogenation can be enhanced by adding 1 wt % Rh to Mo-K/MWCNT catalysts.[18] To the best of our knowledge, the fundamental data on the effect of noble metal on selectivity of Cu-Co based catalysts at typical ethanol synthesis conditions are rather rare.

Generally, the modified catalysts are often characterized by XPS, XRD, TPR, and TEM, *etc.* However, the modification effect between Rh and other elements cannot extensively investigated based on these characterizations. Fortunately, diffuse reflectance infrared Fourier transform spectroscopy (DRIFTS) is a powerful surface-sensitive technique to peer into the adsorption behavior of catalysts under reaction conditions.[19] Moreover, it is helpful to clarify the relation between the adsorption and reaction *via* probe molecule such as CO.[20] However, it was barely reported that DRIFTS was employed to characterize the Cu-Co based catalysts modified by rhodium to date. In this work, the $CuCo/\gamma\text{-}Al_2O_3$ catalysts modified by rhodium were prepared and their CO hydrogenation activities were evaluated. The emphasis of this work is using DRIFTS to investigate the effects of Rh on surface active species in detail.

Experimental

Catalyst Preparation. The supported catalyst samples were prepared by wet impregnation with precursors solutions of cobalt nitrate, copper nitrate and rhodium nitrate on a commercial $\gamma\text{-}Al_2O_3$ (surface area = 256 $m^2\ g^{-1}$, mean pore diameter = 7 nm, 40-60 mesh). After impregnation, the samples were dried at 110 °C for 12 h and then calcined at 500 °C for 4 h in air. For all the catalysts, nominal loading of Cu or Co is 10 wt %. $\gamma\text{-}Al_2O_3$ support is abbreviated as Al_2O_3. A catalyst with Rh loading of 1 wt %, Cu loading of 10 wt %, Co loading of 10 wt % on the $\gamma\text{-}Al_2O_3$ was written as $1Rh\text{-}CuCo/Al_2O_3$.

Catalyst Characterization. The BET surface area, pore

volume and average pore diameter were obtained using N_2 adsorption at −196 °C using a Micrometric ASAP 2020 automated system. Prior to N_2 adsorption, the sample were degassed under vacuum at 120 °C for 6 h. X-ray diffraction (XRD) patterns of the samples were recorded on a Bruker D8 Advance powder diffractormeter, using Cu Kα radiation (λ = 1.54056 Å). Temperature programmed reduction (TPR) measurements were carried out in an AutochemII 2920 instrument. Temperature programmed desorption (TPD) experiments were performed in the same apparatus as used in TPR. X-ray photoelectron spectra (XPS) were recorded over calcined catalysts using a VG ESCALAB 250Xi electron spectrometer equipped with Al Kα X-ray source. The analyzer was operated in a constant pass energy mode, and operated at 10 mA and 12 kV. The binding energies (BE) were referenced to the Al 2p peak. Using this reference, BE values of C 1s peak coming from adventitious carbon appeared at 284.9 ± 0.2 eV. Transmission electron microscopy (TEM) and energy-dispersive X-ray spectroscopy (EDS) measurements were performed using a Tecnal F30 microscope attached an EDX (METEK).

Diffuse reflectance infrared Fourier transform spectroscopy (DRIFTS) experiments were carried out in a Thermo Scientific Nicolet 6700 spectrometer with a PIKE heat chamber. The samples were placed into the infrared cell, which equipped with temperature controlled parts and ZnSe window. The catalyst sample was reduced in H_2 flow at 400 °C for 90 min, and then was flushed with 30 mL min^{-1} N_2 at 410 °C for additional 30 min. Background spectra were collected at different temperatures after the system pressure was evacuated until better than 10^{-3} Pa. The spectra were recorded at 4 cm^{-1} resolution and 128 scans and were collected as N_2 flushed the system for 30 min. Two series of experiments were performed at each temperature: CO adsorption and CO hydrogenation. For CO adsorption experiments, 5% CO/He was introduced to the system for 30 min at a flow rate of 30 mL min^{-1}. For CO hydrogenation reaction, syngas ($CO/H_2/He$ = 5/10/85) was introduced to the system and elevated pressure to 2 MPa. Spectra were collected at 60 °C, 120 °C, 180 °C, 220 °C, 240 °C , 250 °C, and 260 °C using the corresponding background.

Catalytic Activity. CO hydrogenation tests were carried out in a stainless steel continuous flow fixed-bed reactor with internal diameter of 10 mm. The catalyst pellet size was 40-60 mesh. 1 g catalyst was *in situ* reduced under H_2 flow at 400 °C for 10 h before each reaction test. After the reactor was cooled to reaction temperature, the system was pressurized to 2 MPa with syngas ($H_2/CO/N_2$ = 60/30/10) with gas space velocity of 1800 h^{-1}. Prior to be analyzed, the tail gas was passed through a hot trap (180 °C) and a cold trap (0 °C). All the liquid products were collected after 48 h on-stream when the steady state was reached. Tail gas samples were analyzed on-line by two set of GC (Agilent 7890): one is equipped with a TCD to analyze CO, CO_2, N_2 and H_2 using a 5A molecular sieve packed column and a Hayesep Q packed column and the other fitted with FID to separate C_1-C_4 hydrocarbons, oxygenates and water using a HP-PLOT/Q column and a HP-INNOWAX capillary column.

Results and Discussion

XRD, N_2 Adsorption and XPS Results. As can be seen in Figure 1, the XRD patterns of γ-Al_2O_3 exhibits three peaks at 2θ = 36.8°, 45.9° and 67.3°, corresponding to the planes (311), (400) and (440) of γ-Al_2O_3 (JCPDS 29-0063), respectively. Cu/Al_2O_3 shows weak diffraction peaks while Co/Al_2O_3 exhibits apparent diffraction peaks, indicating that the dispersion of Cu is higher than that of Co. CuCo/Al_2O_3 also exhibits three similar intensive peaks with those of Co/Al_2O_3. It is difficult to distinguish $CuCo_2O_4$ or Co_3O_4 species since they have similar peaks at 2θ = 36.74°, 62.85°, and 75.40° (JCPDS 44-1159). Compared with Co/Al_2O_3, CuCo/Al_2O_3 exhibits relative weak diffraction peaks, suggesting that the introduction of Cu is helpful to increase the dispersion of Co. For the Rh modified samples, no peaks of rhodium can be detected owing to the lower Rh loading.[12] Clearly, the diffraction peaks of Co_3O_4/$CuCo_2O_4$ (2θ = 36.74°) was affected by the addition of Rh.

The effects of Rh on the textural characteristics of CuCo/Al_2O_3 were studied by the nitrogen adsorption-desorption and shown in Table 1. It can be seen that only a weak influence presented with the addition of Rh. The XPS spectra of CuCo/Al_2O_3 and Rh promoted CuCo/Al_2O_3 were shown in Figure 2. The Co_3O_4 is generally identified by the binding energy at 780 eV, the spin-orbital splitting and the absence of intense satellite structure. The peaks at about 780.3 eV with low intense satellites were observed for Co 2p XPS spectra and peaks at 931.9 eV for Cu 2p XPS spectra, suggesting the presence of Co_3O_4 and CuO phase in the subsurface layer of the calcined

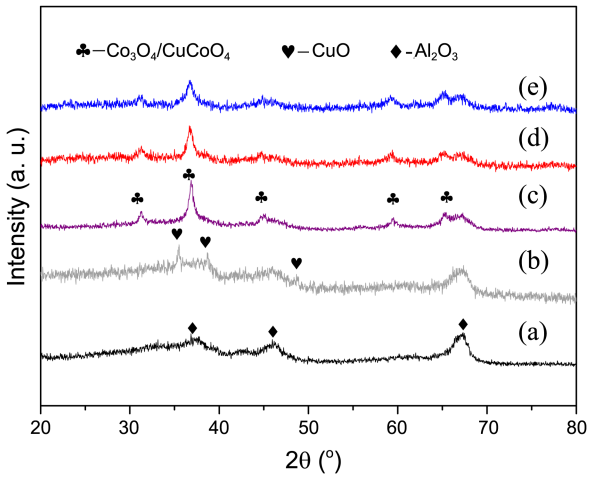

Figure 1. XRD patterns of samples: (a) Al_2O_3, (b) Cu/Al_2O_3, (c) Co/Al_2O_3, (d) CuCo/Al_2O_3, and (e) 1Rh-CuCo/Al_2O_3.

Table 1. Textural properties and compositions of catalysts

Catalysts	S_{BET} (m^2/g)	Cu (%)[a]	Co (%)[a]	Cu/Co[a]
CuCo/Al_2O_3	157	2.4	0.96	2.5
1.0Rh -CuCo/Al_2O_3	164	2.66	0.75	3.54

[a]Determined by XPS

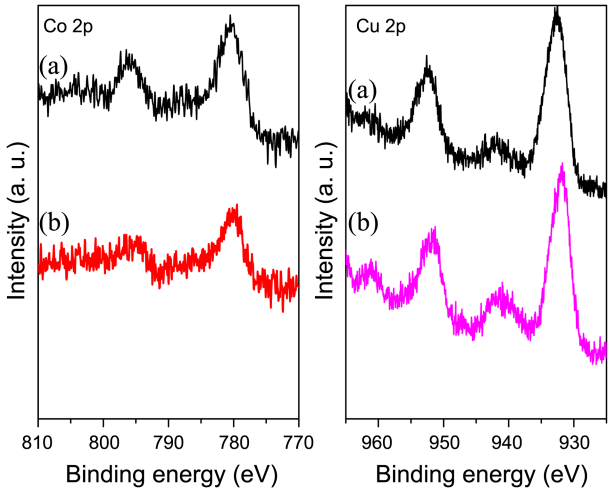

Figure 2. Co 2p and Cu 2p XPS spectra of catalysts: (a) CuCo/Al_2O_3 and (b)1Rh-CuCo/Al_2O_3.

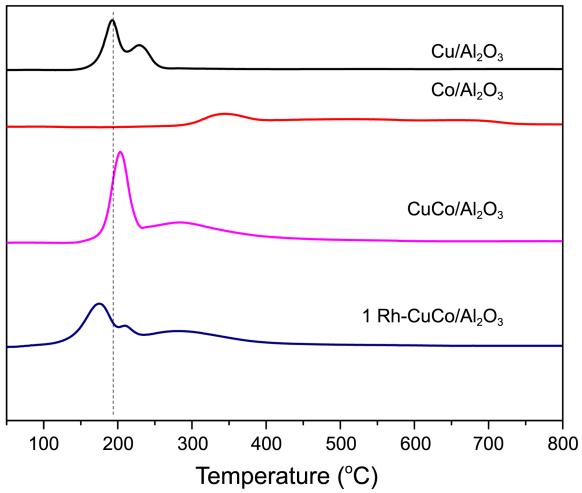

Figure 3. TPR profiles of samples.

catalysts. No significant binding energy shifts were observed in the calcined catalysts, suggesting that rhodium promoters do not alter the chemical state of the surface of calcined catalysts. The surface atomic concentrations of copper and cobalt on the samples were measured by XPS as shown in Table 1. XPS results indicated a much higher surface concentration of copper than cobalt in the calcined catalysts. The addition of 1 wt % Rh further increased the surface concentration of copper. The ratio of Cu/Co surface concentration increases after introduction of Rh, which could provide more active sites for CO insertion.

H_2-TPR. Figure 3 shows the TPR profiles of the calcined catalysts. As can be seen, Cu/Al_2O_3 exhibited one reduction peaks centered at 192 °C with a big shoulder at 231 °C. These two peaks were attributed to the reduction of highly dispersed CuO and Cu_2O respectively. The reduction peak centered at 341 °C and the reduction peak in the range of 400-700 °C for Co/Al_2O_3 could be assigned to the reduction of Co^{3+} to Co^{2+} and Co^{2+} to Co respectively.[21,22] For CuCo/Al_2O_3, the low temperature peak got stronger indicating this peak should be ascribed to the reduction of CuO and Co_3O_4/$CuCo_2O_4$. The high temperature peak in the CuCo/Al_2O_3 was attributed to the reduction of Co_3O_4. After the addition of Rh promoter, the TPR profiles got complicated. A new shoulder peak appeared at right side of low temperature peak. Here, the low temperature peak should be ascribed to the overlapping peak of Rh and CuO since Rh is easily reduced. The shoulder peak may be caused by the reduction of Cu_2O to Cu^0.

***In-situ* DRIFTS Studies.** The surface species and the active sites for CO hydrogenation on the selected catalysts were investigated by DRIFTS. Figure 4 gives the DRIFTS spectra of CO adsorption on catalysts at 60 °C after N_2 purging. For CuCo/Al_2O_3, only one peak at 2112 cm^{-1} could be observed. This peak may be due to linearly adsorbed CO on highly dispersed adsorbed CO on highly dispersed copper sites. After introduction of Rh to CuCo/Al_2O_3, at least one new CO band occurred. The high frequency band showed a slightly red, indicating that a kind of homogeneous copper site formed on the surface due to the addition of Rh.[23] The characteristic bands due to the linear adsorption of CO at Rh^0 sites on the catalyst with 1 wt % Rh were observed at around 2054, 1857 cm^{-1}, which correspond to linear and bridged carbonyl species respectively.[24] The double bands around 2020 and 2010 cm^{-1} usually correspond to the gem-dicarbonyl species on Rh^+.[25] However, the band at 2020 cm^{-1} is absent on 1Rh-CuCo/Al_2O_3, suggesting that this species may overlap with linearly adsorbed CO species on Cu sites.

In order to further investigate the thermal stability of adsorbed species, the DRIFTS experiments on CuCo/Al_2O_3 and 1Rh-CuCo/Al_2O_3 catalysts under CO/He or CO/H_2/He flow at reaction temperature were conducted. Figure 5 shows the DRIFTS spectra during CO/He flow for selected catalysts at reaction temperature. It can be observed that the peak at around 2112 cm^{-1} disappeared at 260 °C for CuCo/Al_2O_3. This band is often attributed to CO adsorbed on Cu^+ (Cu_2O) sites, particularly when it is stable to be heated.[26,27] When easily removable by heating, it has also been assigned to CO

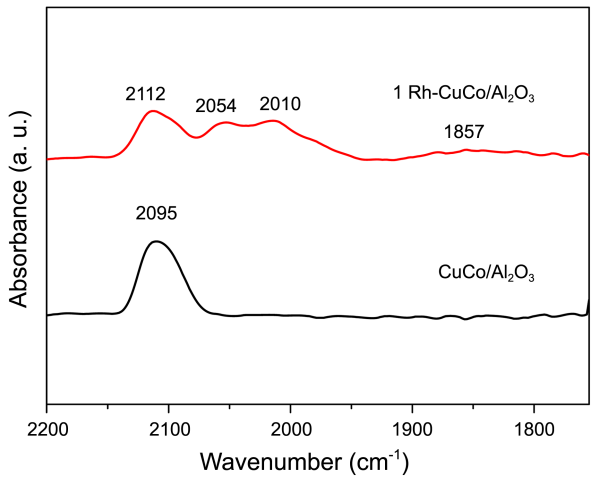

Figure 4. DRIFT spectra of chemisorbed CO over the selected catalysts at 1 atm, 60 °C followed by purging in N_2 flow.

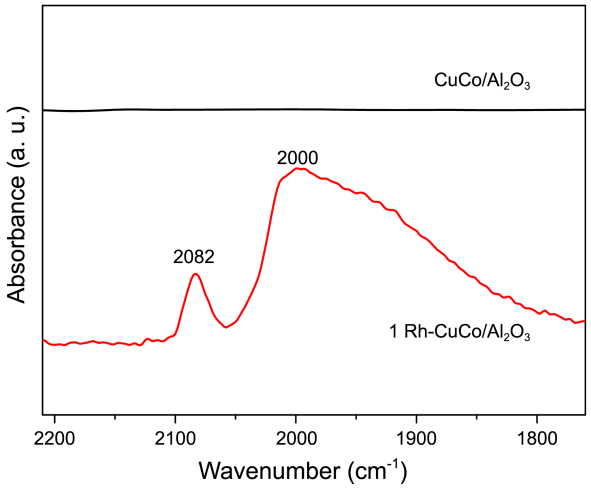

Figure 5. DRIFT spectra of chemisorbed CO over the catalysts at at 1 atm, 260 °C followed by purging in N_2 flow.

adsorbed on small, two-dimensional, partially electropositive copper particles by interacting with oxygen atoms or hydroxyl groups of the support.[28] Some remarkable differences between the DRIFTS spectra of 1Rh-CuCo/Al_2O_3 at 60 °C (Figure 4) and the spectra at reaction temperature (Figure 5) also could be observed. The band centered at 2112 cm^{-1} decreased gradually and shifted to low frequency (2082 cm^{-1}). This band should be accumulation of adsorbed germinal CO on Cu sites. Another observation was that the characteristic bands for Rh^0 disappeared and a broad and strong band around at 2000 cm^{-1} appeared. This indicated that the addition of 1 wt % Rh modified the interaction of CO with copper and/or cobalt.

Figure 6 presents the DRIFTS spectra of CuCo/Al_2O_3 and 1Rh-CuCo/Al_2O_3 under flowing syngas (CO/H_2/He = 5/10/85) at reaction temperature. It can be seen in Figure 6 that the band centered at 2123 cm^{-1}, which is due to CO linearly adsorbed on copper, becomes indistinguishable from gas phase CO at 260 °C for both catalysts. The band located around 2000 cm^{-1} shifted to higher frequency and become more intense for 1Rh-CuCo/Al_2O_3. The former showed that the introduction of Rh increased C-O bond intensity and thus increased non-dissociative CO and the latter indicated this catalyst was more readily dissociated.[29]

DRIFTS investigation of CO+H_2 under reaction pressure (2 MPa) was carried out. Figure 7 and Figure 8 show DRIFT spectra of CuCo/Al_2O_3 and 1Rh-CuCo/Al_2O_3 respectively under syngas flow at temperature ranging from 60 to 260 °C. The bands at 3013, 2967-2932 cm^{-1} (the C-H stretching region) were assigned to the anti-symmetric stretching vibration of CH_2 in M=CH_2, −CH_3 and −CH_2 of surface hydrocarbons respectively.[30] The weak band around 1338 cm^{-1} was assigned to the species of M–CHO (vsCHO).[31] The bands at 1393 cm^{-1}, 1370 cm^{-1} were ascribed to the anti-symmetric and symmetric stretching vibrations of C-O bands (vasOCO and vsOCO) as a result of the HCOO adsorbed on the catalyst surface *via* the hydrogenation of the adsorbed CO_2.[32] The bands of interest in the range of 3550-3750 cm^{-1} were assigned to the stretching vibration of −OH of alcohol.[33,34] It can be observed from Figure 7 that the bands associated with intermediates including –CH_3, –CH_2, −CHO, and −OH became apparent when the temperature is above 240 °C, which implied that dissociative activation of H_2 is one of the crucial steps in ethanol synthesis over the copper/cobalt based catalyst in our experimental conditions. The features of CO hydrogenation on 1Rh-CuCo/Al_2O_3, as shown in Figure 8, were comparable with those of CuCo/Al_2O_3, as follows: the groups –CHO and −OH presents at lower temperature (220 °C) and the peak intensity of them are stronger. This demonstrated that the addition of 1 wt % Rh improved the hydrogenation ability of CuCo catalyst.

H_2-TPD. H_2-TPD can also provide information for hydrogenation ability of the catalysts. As shown in Figure 9, it can be observed that the H_2-TPD peaks of CuCo/Al_2O_3 were presented at around 106 and 550 °C. The intensity of low and high temperature peaks for 1 wt % Rh promoted CuCo/Al_2O_3 are stronger, indicating that the addition of 1 wt % Rh can active H-adspecies. On the other hand, H_2-TPD can be used to judge dispersion of catalysts. As can be seen in

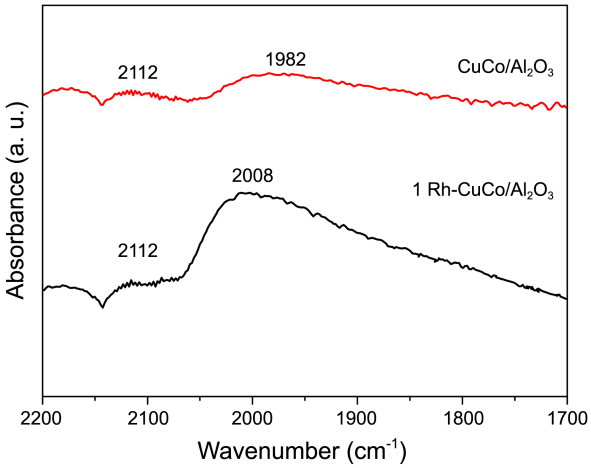

Figure 6. DRIFT spectra during CO/H_2/He flow at 1 atm, 260 °C followed by purging in N_2 flow.

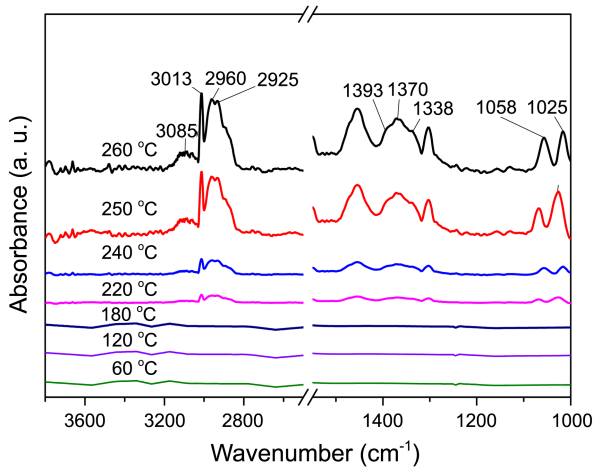

Figure 7. DRIFT spectra of the CuCo/Al_2O_3 during CO hydrogenation at 2 MPa and different temperatures.

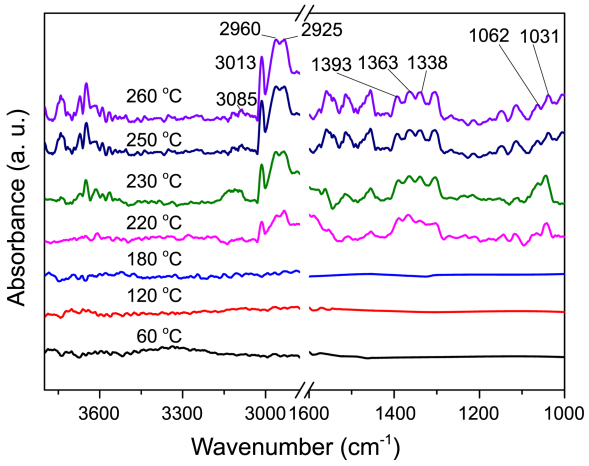

Figure 8. DRIFT spectra of the 1Rh-CuCo/Al_2O_3 during CO hydrogenation at 2 MPa and different temperatures.

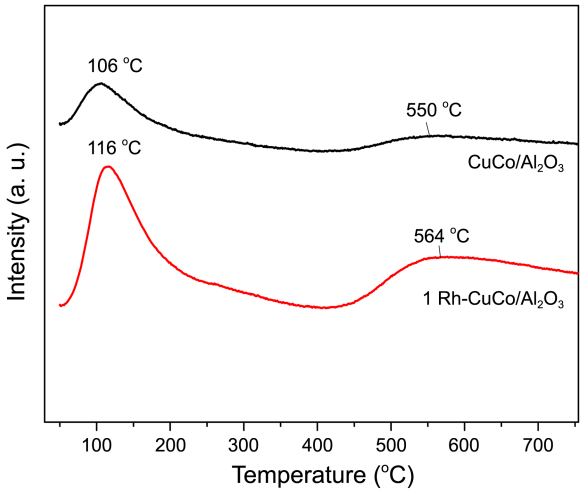

Figure 9. H_2-TPD of catalysts.

Figure 9, the addition of Rh increased dispersion due to both the low and high temperature desorption peak shifted to higher temperature compared to un-promoted CuCo catalysts.

TEM and EDS. EFTEM were carried out to provide additional evidence about dispersion. Figure 10 shows TEM images of reduced catalysts. CuCo/Al_2O_3 sample showed roughly spherical nanoparticles with diameters from 4.5 nm to 20.2 nm. The particle size distribution is narrowed with the addition of 1 wt % Rh and average particle size decrease from 10.5 nm to 8 nm. The larger particles in CuCo/Al_2O_3 have fewer surface atoms that are accessible to CO and H_2 than in 1Rh-CuCo/Al_2O_3 with a smaller particle. The higher selectivity for ethanol using Rh promoted CuCo catalysts could be related to smaller particle size and higher dispersion. EDS (Figure 10(b, d)) on randomly selected points indicated that Cu and Co, Cu, Co and or Rh co-existed in sole nanoparticle, suggesting some interaction would be very likely occurred among these metals.

Catalytic Studies. Table 2 lists the catalytic performances over selected catalysts for the synthesis of ethanol and higher alcohols. The monometallic cobalt catalyst produced mostly

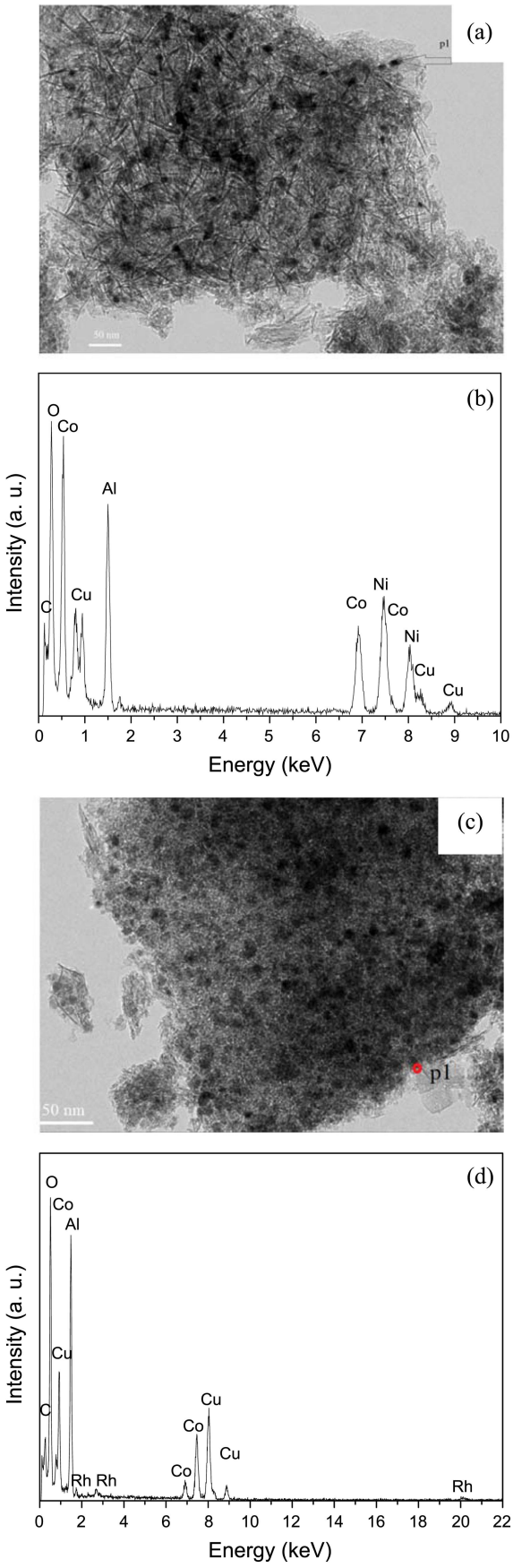

Figure 10. TEM images of (a) CuCo/ Al_2O_3 and (c) 1Rh-CuCo/ Al_2O_3 and corresponding EDS spectra (b, d) of reduced samples.

Table 2. CO hydrogenation performance on different Rh promoted CuCo catalysts[a]

Catalyst	X_{CO}	Selectivity (C %)			$C_{2+}OH^b$ /C_1OH^c
	%	HC	CO_2	ROH	
Cu/Al_2O_3	22.8	26.2	43.2	21.2	0.2
Co/Al_2O_3	45.8	92.4	5.5	2.1	0.52
$CuCo/Al_2O_3$	26.65	75.6	8.79	15.6	1.42
$1Rh\text{-}CuCo/Al_2O_3$	36.74	53.2	13.4	33.6	1.68

[a]Reaction conditions: P=2 MPa, H_2/CO=2, and 1800 h^{-1}). [b]Alcohol with two or more carbons. [c]Methanol

hydrocarbons with only trace concentrations of alcohols. The monometallic copper should exhibit higher activity in methanol synthesis, but it showed higher activity toward CO_2 as seen in Table 2. This may be ascribed to different reduction conditions, pressure and space velocity used in our experiments. Bimetallic $CuCo/Al_2O_3$ showed better higher alcohol selectivity than monometallic catalysts and a moderate conversion between that of Cu/Al_2O_3 and Co/Al_2O_3. It was observed that the incorporation of 1 wt % Rh into the $CuCo/Al_2O_3$ increased CO conversion and ethanol selectivity. The selectivity of total alcohol, ethanol and higher alcohol reached a value of 33.6%, 15.3% and 22.1% respectively on the catalyst with 1 wt % Rh.

Figure 11 shows the product distribution of alcohols. It was observed that major oxygenated products on the catalysts were methanol and ethanol. For the synthesis of higher alcohol over $CuCo/Al_2O_3$, the mass fraction of methanol dominated. However, for $1Rh\text{-}CuCo/Al_2O_3$ catalyst, the mass fraction of alcohol was in order of $C_2H_5OH > CH_3OH > C_3H_7OH > C_4H_9OH > C_5H_{11}OH$. The Anderson-Schulz-Flory (A-S-F) model is a common model to describe the chain growth mechanism. The Anderson-Schulz-Flory (A-S-F) plots for the distribution of alcohols over un-promoted and Rh-promoted CuCo based catalysts were shown in Figure 12. It can be seen in Table 2 that the rhodium addition enhanced the catalytic activity by improving the hydrogenation activity of the system. The chain growth probability calculated over the 1Rh-CuCo catalyst is 0.48, which is higher than that of CuCo catalyst, indicating that the addition of 1 wt % Rh to CuCo based catalyst promoted the chain growth probability and thus increased the reaction rate towards the formation of higher alcohols, with ethanol as a dominant product.

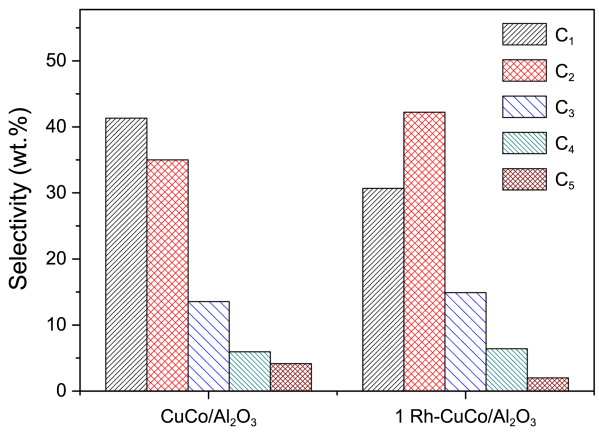

Figure 11. The alcohols product distribution of the catalysts.

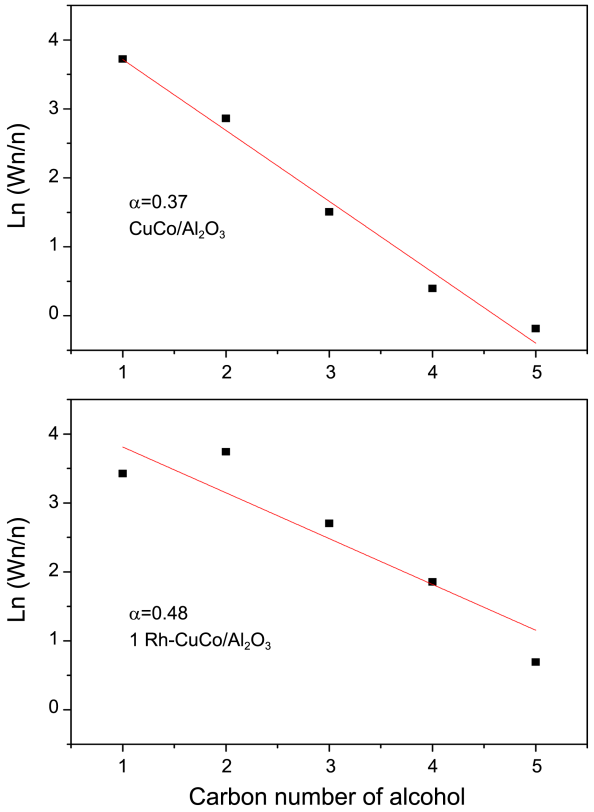

Figure 12. A–S–F plot for the distribution of alcohols over Rh-modified Cu–Co based catalysts.

Conclusions

This study explored the role of Rh in CuCo catalysts for ethanol synthesis. The incorporation of Rh promoter affects the reduction behavior, textual properties, and CO adsorption mode of CuCo based catalysts. The catalyst with 1 wt % Rh exhibited better performance than un-promoted catalysts and showed higher ethanol selectivity at 260 °C and 2 MPa. The alcohol distribution over un-promoted and Rh promoted CuCo catalysts obeys A-S-F rule. 1 wt % Rh promoted $CuCo/Al_2O_3$ presented the higher chain growth probability owing to its better hydrogenation ability manifested by DRIFTS and H_2-TPD. The effect of Rh loading on catalytic activity would be studied in the following work to optimally design an effective catalyst.

Acknowledgments. This work is financially supported by the National Science and Technology Supporting Plan (2006BAE02B02).

References

1. Gong, J.; Yue, H.; Zhao, Y.; Zhao, S.; Zhao, L.; Lv, J.; Wang, S.;

Ma, X. *J. Am. Chem. Soc.* **2012**, *134*, 13922.
2. Gao, J.; Mo, X.; Goodwin, J. G. *J. Catal.* **2009**, *268*, 142.
3. Gogate, M. R.; Davis, R. J. *Chem. Cat. Chem.* **2009**, *1*, 295.
4. Boz, I. *Catal. Lett.* **2003**, *87*, 187.
5. Feng, W.; Wang, Q. W.; Jiang, B.; Ji, P. *Ind. Eng. Chem. Res.* **2011**, *50*, 11067.
6. Xiao, H. C.; Li, D. B.; Li, W. H.; Sun, Y. H. *Fuel. Process Technol.* **2010**, *91*, 383.
7. Christensen, J. M.; Mortensen, P. M.; Trane, R.; Jensen, P. A.; Jensen, A. D. *Appl. Catal. A* **2009**, *366*, 29.
8. O'Shea, V. A; Menéndez, N.; Tornero, J.; Fierro, J. *Catal. Lett.* **2003**, *88*, 123.
9. Panpranot, J.; Goodwin, J. G., Jr.; Sayari, A. *J. Catal.* **2002**, *211*, 530.
10. Aquino, A. D.; Gomez Cobo, A. J. *Catal. Today* **2001**, *65*, 209.
11. Subramanian, N. D.; Balaji, G.; Kumar, C. S. S. R.; Spivey, J. J. *Catal. Today* **2009**, *147*, 100.
12. Wang, J.; Chernavskii, P. A.; Wang, Y.; Khodakov, A. Y. *Fuel.* **2012**, *103*, 1111.
13. Mahdavi, V.; Peyrovi, M. H. *Catal. Commun.* **2006**, *7*, 542.
14. Tsai, Y.-T.; Mo, X.; Goodwin Jr, J. G. *J. Catal.* **2012**, *285*, 242.
15. Xiao, K.; Qi, X.; Bao, Z.; Wang, X.; Zhong, L.; Fang, K.; Lin, M.; Sun, Y. *Catal. Sci. Technol.* **2013**, *3*, 1591.
16. Jacobs, G.; Ji, Y.; Davis, B. H.; Cronauer, D.; Kropf, A. J.; Marshall, C. L. *Appl. Catal. A* **2007**, *333*, 177.
17. Trépanier, M.; Tavasoli, A.; Dalai, A. K.; Abatzoglou, N. *Appl. Catal. A* **2009**, *353*, 193.
18. Surisetty, V. R.; Dalai, A. K.; Kozinski, J. *Appl. Catal. A* **2010**, *381*, 282.
19. Subramanian, N. D.; Kumar, C. S. S. R.; Watanabe, K.; Fischer, P.; Tanaka, R.; Spivey, J. J. *Catalysis Science & Technology* **2012**, *2*, 621.
20. Mo, X. H.; Gao, J.; Umnajkaseam, N.; Goodwin, J. G. *J. Catal.* **2009**, *267*, 167.
21. Chu, W.; Chernavskii, P. A.; Gengembre, L.; Pankina, G. A.; Fongarland, P.; Khodakov, A. Y. *J. Catal.* **2007**, *252*, 215.
22. Karaca, H.; Safonova, O. V.; Chambrey, S.; Fongarland, P.; Roussel, P.; Griboval-Constant, A.; Lacroix, M.; Khodakov, A. Y. *J. Catal.* **2011**, *277*, 14.
23. Xu, R.; Yang, C.; Wei, W.; Li, W. H.; Sun, Y. H.; Hu, T. D. *J. Mol. Catal. A: Chem.* **2004**, *221*, 51.
24. Basu, P.; Panayotov, D.; Yates, J. T. *J. Am. Chem. Soc.* **1988**, *110*, 2074.
25. Chuang, S. S. C.; Stevens, R. W.; Khatri, R. *Top Catal.* **2005**, *32*, 225.
26. Hadjiivanov, K.; Tsoncheva, T.; Dimitrov, M.; Minchev, C.; Knözinger, H. *Appl. Catal. A* **2003**, *241*, 331.
27. Tsoncheva, T.; Venkov, T.; Dimitrov, M.; Minchev, C.; Hadjiivanov, K. *J. Mole. Catal. A* **2004**, *209*, 125.
28. Smith, M. L.; Kumar, N.; Spivey, J. J. *J. Phys. Chem. C* **2012**, *116*, 7931.
29. Subramanian, N. D.; Gao, J.; Mo, X. H.; Goodwin, J. G.; Torres, W.; Spivey, J. J. *J. Catal.* **2010**, *272*, 204.
30. Fukushima, T.; Arakawa, H.; Ichikawa, M. *J. Phys. Chem.* **1985**, *89*, 4440.
31. Raskó, J.; Kecskés, T.; Kiss, J. *J. Catal.* **2004**, *226*, 183.
32. Li, C.; Domen, K.; Maruya, K.-I.; Onishi, T. *J. Catal.* **1990**, *125*, 445.
33. Edwards, J. F.; Schrader, G. *J. Phys. Chem.* **1984**, *88*, 5620.
34. Yang, X. M.; Wei, Y.; Su, Y. L.; Zhou, L. P. *Fuel. Process Technol.* **2010**, *91*, 1168.